

Vision-based adaptive control of a 3-RRR parallel positioning system

YAO Sheng, LI Hai, ZENG Lei & ZHANG XianMin*

Guangdong Key Laboratory of Precision Equipment and Manufacturing Technology, School of Mechanical and Automotive Engineering, South China University of Technology, Guangzhou 510640, China

Received August 17, 2017; accepted December 14, 2017; published online January 19, 2018

The macro positioning stage with high-precision and rapid positioning ability plays a crucial role in the macro-micro combination positioning system. In this paper, we develop a practical method for the control of a 3-RRR planar positioning system using online vision measurement as feedback. In this method, a monocular vision system is established to accomplish high-precision online pose measurement for the 3-RRR manipulator. Additionally, a robust and operable adaptive control algorithm, which incorporates a fuzzy controller and a PI controller, is employed to achieve precise and rapid positioning of the 3-RRR positioning system. A series of experiments are conducted to verify the positioning performances of the proposed method, and a conventional PI control algorithm is utilized for comparison. The experimental results indicate that using the proposed control approach, the parallel positioning system obtains high precision and shows higher efficiency and robustness, especially for the time-varying positioning system.

adaptive positioning control, 3-RRR planar parallel manipulator, machine vision-aided system, full-closed loop control

Citation: Yao S, Li H, Zeng L, et al. Vision-based adaptive control of a 3-RRR parallel positioning system. *Sci China Tech Sci*, 2018, 61, <https://doi.org/10.1007/s11431-017-9181-9>

1 Introduction

In recent years, much attention has been drawn to the field of precision positioning systems. For example, an automated macro robot combined with a three degree-of-freedom (DOF) nano positioning platform for the nano manipulation of carbon nanotubes is developed by Fatikow et al. [1], a 3D micro operating system with two serial robot units is designed by Gupta et al. [2], and the concept of “lab in scanning electron microscope (SEM)” based on a serial positioning platform is proposed by Fahlbusch et al. [3]. Nevertheless, few positioning systems can achieve the goal of both decimeter-scale workspace and nanoscale accuracy.

The macro-micro combination positioning system plays a significant role in the field of precision manipulation. This

type of system usually consists of compliant mechanisms as the micro positioner, which can meet the requirements of high precision positioning and multiple DOFs but are not able to perform large-scale positioning [4,5]. To solve this problem, the macro part of the macro-micro combination positioning system is designed to fulfill the requirements of large-stroke positioning. Moreover, compared with serial robots, which are generally used in recent research studies, parallel robots have the virtues of higher speed, stronger load capacity and better precision with small accumulative errors [6–9]. Accordingly, the planar parallel manipulator (PPM) is capable of loading the micro positioner and is suitable as the macro part of this combination system. Generally, the positioning error of the macro part should be smaller than the workspace of the micro part to allow the micro part to complete the final positioning and achieve high accuracy. Thus, the positioning accuracy of the macro positioning

*Corresponding author (email: zhangxm@scut.edu.cn)

system is particularly important and can be improved by control algorithms [10,11]. Because the PPM is affected by the nonlinear factors (such as friction clearance and elastic deformation in transmission) and the uncertain factors of the environment (such as noise), it is a challenge to control the parallel precision positioning system in practical use.

All the control methods of parallel precision positioning systems can be roughly classified as open-loop control, semi-closed loop control, and full-closed loop control. While the open-loop control is easily affected by external interference, the semi-closed loop control is the most common control method for PMs because of its low cost; however, because of the lack of feedback at the end-effector, its control performances are always influenced by the manufacturing, assembly errors and deformation of PMs. Therefore, the full-closed loop control is a more effective and ideal control method; however, its accuracy is relevant to measuring auxiliary devices, such as laser displacement sensors [12], acceleration sensors [13,14], and machine vision systems [15–17]. The PID (proportion integration differentiation) type control has been widely used because of its robustness and stability. Cheng et al. [18] compared control performances of 2-DOF PPMs based on four types of PD control. Yong et al. [19] established a full-closed loop control system for 3-RRR PPM based on eddy current sensors utilizing the conventional PI control algorithm. However, those classic PID algorithms have poor control performance for nonlinear, time-varying, and uncertain systems. The coupling and inconvenient adjustment of PID parameters are also regarded as disadvantages. In recent years, some researchers, such as Ren et al. [20] recommend intelligent control schemes for planar positioning systems; Vermeiren et al. [21] designed different fuzzy control methods for several parallel robot systems. Other researchers such as Cong et al. [13,14] focused on developing the dynamic acceleration feedback controller and the adaptive computed torque controller based on the dynamic model of the parallel manipulators; Wu et al. [22–25] also presented several dynamic control strategies of the parallel manipulators, especially for the applications in machine tools.

The most common architecture for a 3-DOF PPM is the 3-RRR architecture (R represents the revolute pair), which is easy to manufacture and has a larger workspace [26]. To the best knowledge of the authors, few literatures have been presented for the adaptive control of a 3-RRR type macro positioning system utilizing the machine vision method in the design of the macro-micro combination positioning system. In this paper, we describe a practical macro positioning system for the coarse positioning of the nano manipulation using the adaptive control method with assistance from a monocular vision system. A 3-RRR positioning system including a 3-RRR PPM and the vision aided system is established in Section 2. In Section 3, an adaptive control

method that combines the fuzzy controller and the PI controller is developed for precise positioning. Finally, a series of experiments are conducted and presented to demonstrate the effectiveness of the proposed method.

2 Modeling of the 3-RRR positioning system

The 3-RRR positioning system is designed as the macro part of macro-micro combination positioning system. The positioning accuracy of the macro part must meet the requirement that its positioning error is much smaller than the workspace of the micro positioner, as a result, the precision of the 3-RRR positioning system requires improvement, and it is necessary to investigate the control method. First, the model of 3-RRR positioning system should be established because such a model is essential for the position control of the parallel robots. Moreover, to provide feedback from the end-effector, an online machine vision system is set up, as described in this section.

2.1 Inverse kinematics modeling

Solving the inverse kinematics is necessary because the parallel robot tasks are popularly formulated according to the position and motion of the end-effector.

The 3-RRR PPM consists of a static platform, a moving platform and three branches of kinematic chains. As shown in Figure 1, the static platform refers to the plant of $A_1A_2A_3$. The moving platform refers the equilateral triangle $C_1C_2C_3$, which is also regarded as the end-effector. On the static platform, the global Cartesian coordinate system OXY is established, where O is the centroid of the static platform. Similarly, the moving coordinate system $O'X'Y'$ is established on the moving platform, where O' is the centroid of the end-effector $C_1C_2C_3$. A_1 , A_2 and A_3 also can represent three actuated joints, which are fixed to the base, and together with the other six unactuated joints (B_1 , B_2 , B_3 , C_1 , C_2 , C_3) form three closed kinematic chains. Thus, the vector $O'O$ can be defined as the position of the end-effector (x , y , ϕ).

As shown in Figure 2, a single branch of the kinematic chain and the end-effector can form the closed-loop vector $\mathbf{O}-\mathbf{A}_i-\mathbf{B}_i-\mathbf{C}_i-\mathbf{O}'-\mathbf{O}$. Based on the closed loop vector method [27,28], the following equation is obtained:

$$\mathbf{O}\mathbf{A}_i + \mathbf{A}_i\mathbf{B}_i + \mathbf{B}_i\mathbf{C}_i + \mathbf{C}_i\mathbf{O}' + \mathbf{O}\mathbf{O}' = \mathbf{0} \quad (i=1, 2, 3). \quad (1)$$

For convenience we define $\mathbf{O}\mathbf{A}_i$ as \mathbf{d}_i ; $\mathbf{O}'\mathbf{C}_i$ as \mathbf{h}_i ; and $\mathbf{O}\mathbf{O}'$ as \mathbf{r} . The length of drive rod $\mathbf{A}_i\mathbf{B}_i$ is a_i and the orientation is θ_i ; the length of follower rod $\mathbf{B}_i\mathbf{C}_i$ is b_i and its unit vector is \mathbf{n}_i . Thus, that eq. (1) can be rewritten as

$$\mathbf{r} = \mathbf{d}_i + \mathbf{R}_{\theta_i}a_i\mathbf{e}_1 + b_i\mathbf{n}_i - \mathbf{R}_{\phi}\mathbf{h}_i, \quad (2)$$

where

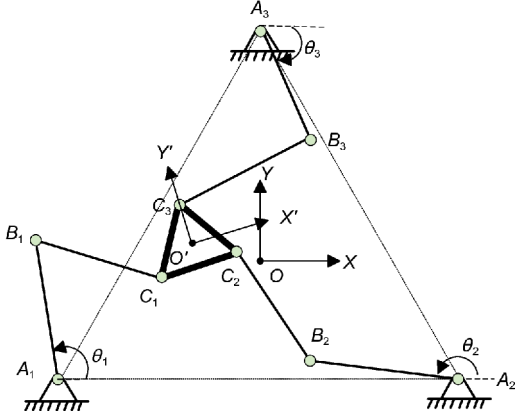


Figure 1 Schematic of the 3-RRR PPM.

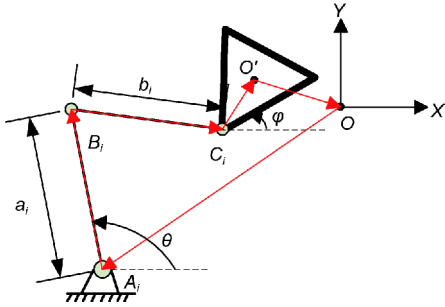


Figure 2 (Color online) Closed loop vector of a branch.

$$\mathbf{R}_{\theta_i} = \begin{pmatrix} \cos\theta_i & -\sin\theta_i \\ \sin\theta_i & \cos\theta_i \end{pmatrix}, \mathbf{R}_\varphi = \begin{pmatrix} \cos\varphi & -\sin\varphi \\ \sin\varphi & \cos\varphi \end{pmatrix},$$

$$\mathbf{e}_1 = \begin{pmatrix} 1 \\ 0 \end{pmatrix}.$$

Through 2-norm processing, a new equation is obtained:

$$\|\mathbf{r} - \mathbf{d}_i - \mathbf{R}_{\theta_i} a_i \mathbf{e}_1 + \mathbf{R}_\varphi \mathbf{h}_i\|_2 = \|b_i \mathbf{n}_i\|_2. \quad (3)$$

According to the established coordinate system, the following formulas are obtained:

$$\mathbf{r} = (x, y); \quad \mathbf{d}_i = (d_i \cos\alpha_i, d_i \sin\alpha_i);$$

$$\mathbf{h}_i = (h_i \cos\beta_i, h_i \sin\beta_i);$$

$$\boldsymbol{\alpha} = [7\pi/6, 11\pi/6, \pi/2]; \quad \boldsymbol{\beta} = [7\pi/6, 11\pi/6, \pi/2],$$

which lead to

$$\begin{aligned} & (x + \mathbf{h}_i \cos(\beta_i + \varphi) - \mathbf{d}_i \cos(\alpha_i) - a_i \cos(\theta_i))^2 \\ & + (y + \mathbf{h}_i \sin(\beta_i + \varphi) - \mathbf{d}_i \sin(\alpha_i) - a_i \sin(\theta_i))^2 = b_i^2. \end{aligned} \quad (4)$$

Eq. (4) can also be written as

$$A_i \sin(\theta_i) + B_i \cos(\theta_i) + C_i = 0. \quad (5)$$

By solving eq. (5), the equation of input and output is obtained as

$$\theta_i = 2\arctan\left(\frac{-A_i \pm \sqrt{A_i^2 + B_i^2 - C_i^2}}{C_i - B_i}\right), \quad (6)$$

where

$$A_i = -2a_i[y + \mathbf{h}_i \sin(\beta_i + \varphi) - \mathbf{d}_i \sin(\alpha_i)];$$

$$B_i = -2a_i[x + \mathbf{h}_i \sin(\beta_i + \varphi) - \mathbf{d}_i \sin(\alpha_i)];$$

$$C_i = [y + \mathbf{h}_i \sin(\beta_i + \varphi) - \mathbf{d}_i \sin(\alpha_i)]^2 + [x + \mathbf{h}_i \sin(\beta_i + \varphi) - \mathbf{d}_i \sin(\alpha_i)]^2 + a_i^2 - b_i^2.$$

In terms of eq. (6), we obtain the angles of actuated joints from the position and orientation of the end-effector.

2.2 Velocity inversion

To control the 3-RRR PPM, not only the position and pose angle but also the speed and angular velocity of the end-effector should be considered. The Jacobian matrix is a mathematical expression that describes the transformation relationship between the vector of actuated joint velocities and the vector of end-effector velocities in Cartesian space. The Jacobian matrix can be determined as

$$\mathbf{J}\dot{\boldsymbol{\theta}} = \dot{\mathbf{X}}. \quad (7)$$

By differentiating eq. (4), the following equation is obtained:

$$\mathbf{D}\dot{\boldsymbol{\theta}} = \mathbf{E}\dot{\mathbf{X}}, \quad (8)$$

where

$$\mathbf{D} = \begin{bmatrix} D_{11} & 0 & 0 \\ 0 & D_{22} & 0 \\ 0 & 0 & D_{33} \end{bmatrix}; \quad \dot{\boldsymbol{\theta}} = \begin{bmatrix} \dot{\theta}_1 \\ \dot{\theta}_2 \\ \dot{\theta}_3 \end{bmatrix};$$

$$\mathbf{E} = \begin{bmatrix} E_{11} & E_{12} & E_{13} \\ E_{21} & E_{22} & E_{23} \\ E_{31} & E_{32} & E_{33} \end{bmatrix}; \quad \dot{\mathbf{X}} = \begin{bmatrix} \dot{x} \\ \dot{y} \\ \dot{\varphi} \end{bmatrix};$$

$$D_{ii} = \frac{1}{2}(B_i \sin\theta_i - A_i \cos\theta_i);$$

$$E_{i1} = -B_i / (2\alpha_i) - \alpha_i \cos\theta_i;$$

$$E_{i2} = -A_i / (2\alpha_i) - \alpha_i \sin\theta_i;$$

$$E_{i3} = E_{i1} h_i \sin(\varphi + \alpha_i) - E_{i2} h_i \cos(\varphi + \alpha_i),$$

$$(i = 1, 2, 3).$$

Therefore, the Jacobian matrix of the 3-RRR PPM is

$$\mathbf{J} = \mathbf{D}^{-1} \mathbf{E}. \quad (9)$$

2.3 Online vision-aided system modeling

Compared with other traditional methods, the visual servo control is a non-contact measuring method that uses visual information as feedback, thereby improving the flexibility and operability of a parallel robot system.

In our proposed control method, we use an monocular vision system to measure the pose of the end-effector by recognizing its low-level geometric feature. Generally, point features are more widely used in vision-aided pose mea-

surement. Although two mark points are sufficient because 3-RRR PPM only moves in a plane, the use of more markers will improve the robustness of the visual measurement. Hence, we use three mark points in our vision system. As shown in Figure 3, four coordinate systems are established. XYZ is the static coordinate based on the static platform. $X'Y'Z'$ is the coordinate on the moving platform, which is also at the plane of the mark points. UV is the image coordinate, and its origin is located at the top-left corner. $X_c Y_c Z_c$ is the camera coordinate, and its origin O_c also represents the optical center. SP, MP and IP are abbreviation for the static plane, moving plane and image plane, respectively. h , d and f represent the distances of SP-MP, MP-IP and the focal length of the lens, respectively.

Based on the pin-hole model [29], the projective transformation equation is obtained as

$$\begin{pmatrix} u \\ v \\ 1 \end{pmatrix} = s\mathbf{K}[\mathbf{R}, \mathbf{T}] \begin{pmatrix} x \\ y \\ z \\ 1 \end{pmatrix}, \quad (10)$$

where s is an arbitrary factor, \mathbf{K} signifies the camera intrinsic parameter matrix, \mathbf{R} represents the rotation matrix, and \mathbf{T} represents the translation vector. (u, v) represents the image coordinate, and (x, y, z) signifies the world coordinate. This is also known as the perspective-n-points method (PnP).

Because, on the moving platform of the 3-RRR PPM, Z -axis is parallel to the optical axis, and SP, MP and IP are parallel to each other, eq. (10) can be simplified as follows:

$$\begin{pmatrix} u \\ v \\ 1 \end{pmatrix} = s\mathbf{KA} \begin{pmatrix} x \\ y \\ 1 \end{pmatrix} = s\mathbf{K} \begin{pmatrix} \cos\theta & -\sin\theta & t_x \\ -\sin\theta & -\cos\theta & t_y \\ 0 & 0 & t_x \end{pmatrix} \begin{pmatrix} x \\ y \\ 1 \end{pmatrix}, \quad (11)$$

where \mathbf{A} is a simplified transformation matrix. We call this equation the degenerated perspective-n-points model (DPnP).

According to eq. (11), the actual pose can be acquired by calculating the static coordinate from image coordinate. This vision-aided method has highly efficient performance and can achieve online processing. Moreover, the measuring accuracy of this machine vision method can be improved by calibrating. Hence, this practical and reliable vision-aided system can be used to provide feedback for the 3-RRR positioning system.

Generally, in the 3-RRR positioning system, the end-effector can move to any target position inside the workspace by the control of motion controller. The actual pose of the end-effector can be measured by the camera and sent to the motion-controller straightaway. Thus, the full-closed loop control system is established; more details regarding the parameters of this system are presented in Section 4. The setup of the 3-RRR positioning system is drawn in Figure 4.

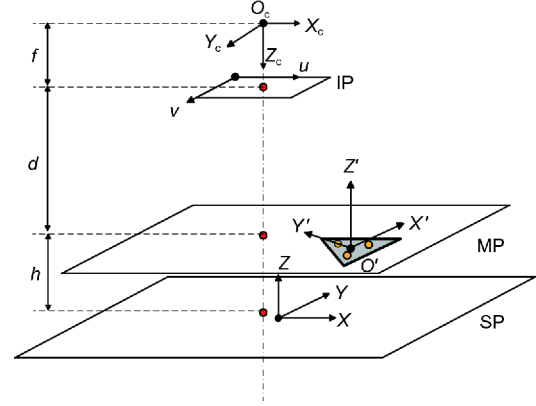


Figure 3 (Color online) Coordinate frames of the vision-aided positioning system.

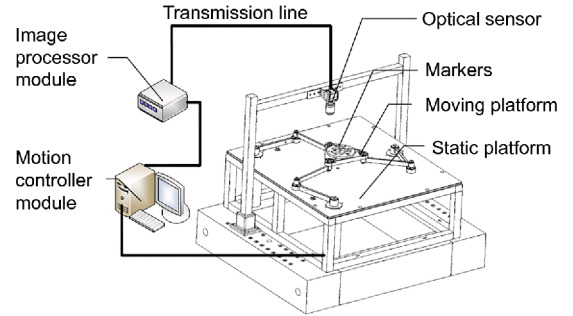


Figure 4 Setup of the 3-RRR positioning system.

3 Control strategy

Most of the PPM control systems are based on semi-closed loop control, i.e., the pose of the end-effector is estimated only through the direct kinematics model. However, for practical applications, the elastic deformation of linkages, the wear of the bearing seat and some non-geometric parameters, such as gear clearances and joint clearance, are inevitable. In these circumstances, the kinematic model has a time-varying property. Thus, estimating the pose of the end-effector through the kinematics model may cause large positioning error, which cannot meet the demand of coarse positioning in the macro-micro combination system. To ensure and improve positioning accuracy, a full-closed loop control system is developed based on the online vision-aid method, and an adaptive control algorithm based on machine vision is proposed.

3.1 Online measuring algorithm

The steps of the online measuring algorithm are listed as follows:

Step 1. A proposed calibration method [30] is utilized for the camera calibration. To ensure that the angle between BP

and IP is as small as possible, the tilt angle can be controlled through camera calibration.

Step 2. Hand-eye calibration is conducted to transfer the pose from the image coordinate to the static coordinate through the DPnP method.

Step 3. After the image of the pose is acquired, it will be processed by three main steps—a threshold segmentation step, a connected component analysis step and a center of gravity step.

Step 4. The pose is calculated through the DPnP model, and its results are sent to the motion controller as feedback. This procedure is shown in Figure 5.

3.2 Full-closed loop control system

To improve the response speed and the accuracy of the rotated actuated joints, servo motors are used to drive the 3-RRR PPM. Moreover, through the rotary encoder on the motor output shaft, the semi-closed loop control is formed to ensure the accuracy of input.

To improve the positioning accuracy of the end-effector, the full-closed loop control system is set up as shown in Figure 6. A high-precision pose measuring sensor, which is an optical camera in this paper, is able to acquire real-time images of the pose and send them to the industrial personal computer (IPC) as feedback through an image processor. When the actual positioning error is larger than the preset threshold, the IPC will calculate input compensations based on the control algorithms. After the compensation is completed, the optical camera will measure the pose of the end-effector again. This procedure repeats continuously until the positioning error is smaller than the preset threshold.

3.3 Adaptive fuzzy control law

The PID control algorithm is widely utilized in motion control because of its advantages, such as simple structure, high robustness, and easy of implementation. Although the conventional PID algorithm is a linear method, it is still able to compensate for weak nonlinearity.

In actual motion control, the continuous PID control algorithm should be transformed into a digital PID algorithm because it requires some time for sampling, analysis, and processing of data. The positional digital PID control algorithm is expressed as

$$u(k) = K_p e(k) + K_I T \sum_{j=1}^k e(j) + \frac{K_D}{T} [e(k) - e(k-1)], \quad (12)$$

where $e(k)$ is the feedback error, K_p , K_I and K_D are the coefficients of the proportional, integral and differential respectively, T is the sampling period, and k is the sampling number. To reduce the adapting time and improve the anti-interference ability, K_D is discarded, and eq. (12) is modified

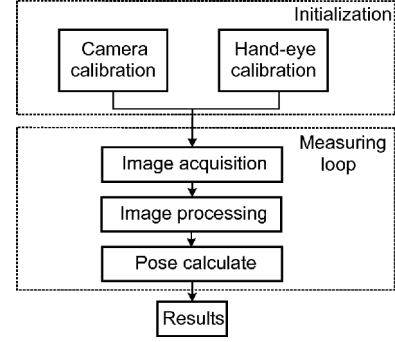


Figure 5 Flow diagram of the online measurement algorithm.

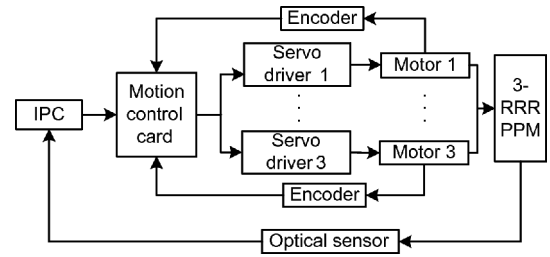


Figure 6 Flow diagram of the full-closed loop control system.

into eq. (13).

$$u(k) = K_p e(k) + K_I T \sum_{j=1}^k e(j). \quad (13)$$

The conventional PI method may achieve good control performance only when the control model is determined and accurate, especially after the calibration of the 3-RRR PM. As time passes, the control model will change via the time-varying property and the uncertainty of the system. Thus, the parameters of the PI method must be reset both appropriately and frequently. Aiming at solving this problem, an adaptive compensation algorithm of the 3-RRR positioning system is adopted.

The fuzzy control algorithm utilizes natural language rules to achieve rough control of the system. If the system only uses fuzzy controllers, then the time required for point stabilization is generally longer than the time required by the conventional PI controllers. Thus, to make full use of the advantages of the conventional PI control algorithm, a fuzzy controller is added to the control structure, and the compensation value is adjusted adaptively. The adaptive fuzzy control system of the 3-RRR positioning system is constructed as illustrated in Figure 7. The fuzzy controller corrects the structural parameters of the conventional PI controller, to ensure that the PI controller is always in the best state at all moments, and the regulation time of the control system is shortened.

The input of the fuzzy controller includes error e , its first derivative $ec=de/dt$, second derivative $ecc=d^2e/dt^2$ and so on. However, increasing the inputs will worsen the real-time

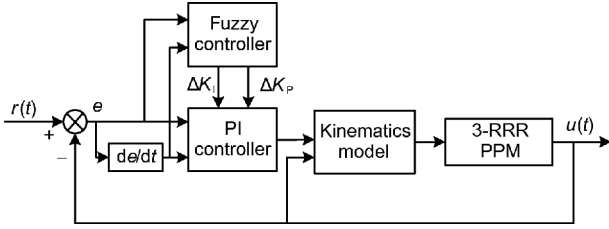


Figure 7 Schematic diagram of the adaptive fuzzy control law.

performance of the control system. Thus, we select error e , and its first derivative $ec=de/dt$ as two-dimensional inputs of the fuzzy controller; the basic composition of the fuzzy controller is shown in Figure 8.

The design procedure of the fuzzy controller is described as follows:

Step 1. Domain transformation. The two-dimensional inputs of the controller normally have different ranges of values. To simplify the controller design, these two different ranges are transformed into the same range by the fuzzy domain.

The value ranges of error e and its first derivative ec are defined as $[-e_1, e_1]$ and $[-ec_1, ec_1]$ respectively. $[-n, n]$ signifies the fuzzy domain. The domain conversion coefficients k_e and k_{ec} can be obtained by eqs. (14) and (15), respectively.

$$k_e = \frac{n}{e_1}, \quad (14)$$

$$k_{ec} = \frac{n}{ec_1}. \quad (15)$$

Similarly, for the output, a fixed fuzzy domain is transferred to respective ranges by multiplying the corresponding domain conversion coefficients.

Step 2. Fuzzifier. The fuzzy domain is divided into five fuzzy subsets denoted as Negative Big (NB), Negative Small (NS), Zero (Z), Positive Small (PS) and Positive Big (PB). We select $[-4, 4]$ as the fuzzy domain for the convenience of programming. As shown in Figure 9, except for points $x=-4, -2, 0,$ and 2 , all points are members of two fuzzy subsets.

Step 3. Inference mechanism. The inference mechanism is the core of the fuzzy controller. First, the fuzzy language rules between outputs $(\Delta K_p, \Delta K_1)$ and inputs (e, ec) are established. Next, according to the approximate reasoning theory and the membership state of e and ec , the fuzzy set of

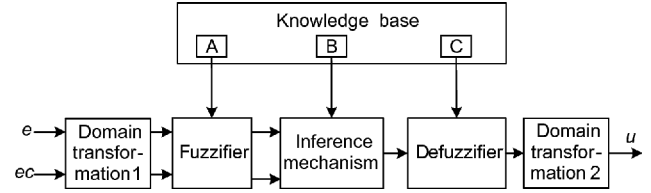


Figure 8 The basic composition of fuzzy controller.

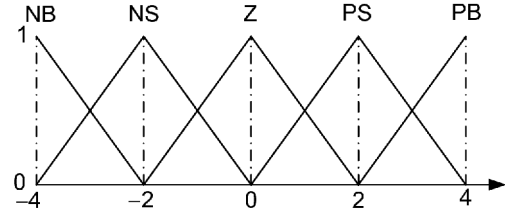


Figure 9 Membership function.

parameter correction $(\Delta K_p, \Delta K_1)$ is obtained. Basically, the rule of the inference mechanism is summarized up by the experience and analysis of actual control. Such a rule can be described as follows: when the absolute value of the error e is large, a larger value of K_p should be selected to improve the response speed of the system. Correspondingly, to prevent excessive overshoot, a smaller ΔK_1 should be chosen. When the value of e is small and the value of ec is large, larger values of both K_p and K_1 should be taken to decrease the systematic static error.

One important feature of fuzzy control is that it can produce a control strategy based on the expert knowledge of a process. Based on the experience that the author summarizes in debugging the system, the fuzzy rules for the 3-RRR positioning system is present in Tables 1 and 2, and Figures 10 and 11. According to the tables, there are 25 different combinations among $e, ec, K_p,$ and K_1 . Except for some points mentioned above, all points belong to two fuzzy subsets. Thus, there are at most 4 different combinations for each input in this fuzzy controller.

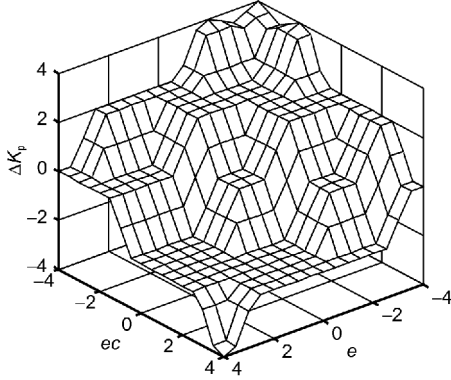
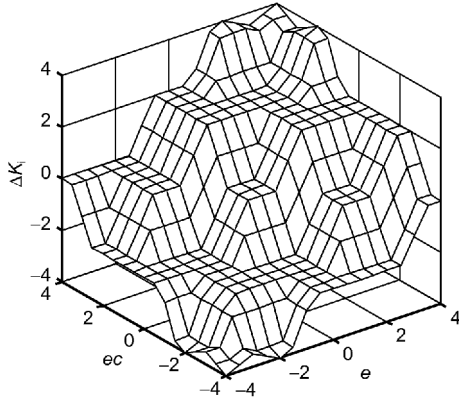
Step 4. Defuzzifier. After the inputs the processed by the inference mechanism module, a fuzzy set is obtained, which cannot be used as the controlled variables directly. Hence, this fuzzy set must be defuzzified. In this paper, the max-

Table 1 Fuzzy rule of ΔK_p

ΔK_p		ec				
		NB	NS	Z	PS	PB
e	NB	PB	PB	PS	PS	Z
	NS	PB	PS	PS	Z	NS
	Z	PS	PS	Z	NS	NS
	PS	PS	Z	NS	NS	NS
	PB	Z	Z	NS	NS	NB

Table 2 Fuzzy rule of ΔK_1

ΔK_1		ec					
		NB	NS	Z	PS	PB	
e	NB	NB	NB	NS	NS	M	
	NS	NB	NS	NS	Z	Z	
	Z	NS	NS	Z	PS	PS	
	PS	NS	Z	PS	PS	PB	
	PB	Z	PS	PS	PB	PB	

**Figure 10** The output surface of ΔK_p .**Figure 11** The output surface of ΔK_1 .

imum membership principle [31] is utilized in the defuzzifier of the fuzzy controller. Based on this principle, the largest membership degree of the fuzzy set members is selected and considered as the outputs of the defuzzifier. If there are many members that have the largest membership degree jointly, then their average value will be taken as the output of the defuzzifier instead.

Bounded-input and bounded-output (BIBO) stability is a form of stability for systems that take inputs. If a system is BIBO stable, then the output will be bounded for every input to the system that is bounded. In our fuzzy system, the following can be obtained:

$$\begin{aligned}
 \Delta u &= \Delta u_1(k) - u_2(k-1) \\
 &= K_p(k) \left(1 + \frac{\Delta t}{T_i} \right) e(k) - K_p(k) e(k-1) \\
 &\leq K_p(k) \left(1 + \frac{\Delta t}{T_i} \right) + v_1 e_{\max}, \quad (16)
 \end{aligned}$$

where

$$\begin{aligned}
 e_{\max} &= \max(e(0), e(1), e(2), \dots, e(k-1)), \\
 v_1 &= \max(K_p).
 \end{aligned}$$

Because $\|g \cdot (u(k))\| \leq \|g\| \cdot u(k)$, the sufficient condition of BIBO stability is $K_p \left| 1 + \frac{\Delta t}{T_i} \right| \cdot \|g\| < 1$, which our control algorithm achieves. Therefore, our proposed control method is stable in theory [32,33].

4 Experiments and analysis

To verify the reliability and practicability of the proposed adaptive control method, a 3-RRR positioning system with vision-aided devices is established, and a series of experiments are performed. The first part is conducted to show the performance and effectiveness of the proposed method. The second part is used to compare the proposed method with the conventional PI method.

4.1 Introduction of the experimental setup

A 3-RRR PPM is manufactured based on an optimum design proposed in the author's previous article [34]. The length parameters of this 3-RRR PPM are $a_i=245$ mm, $b_i=242$ mm, $h_i=112$ mm, $d_i=400$ mm ($i=1, 2, 3$). Figure 12 shows the workspace and its corresponding inscribed circles of the 3-RRR PPM. The workspace is a triangular-like region, and the radius of its inscribed circle is $a_i+b_i+h_i-d_i=199$ mm. In either real practical application or our experiment, the PPM would not be operated in the whole workspace because the performances of the PPM would become worse if the end-effector is closer to the workspace boundary. Based on the vision field of the vision-aided system, a square area with the dimension 150 mm×150 mm is selected in this study.

The experimental apparatus of the 3-RRR positioning

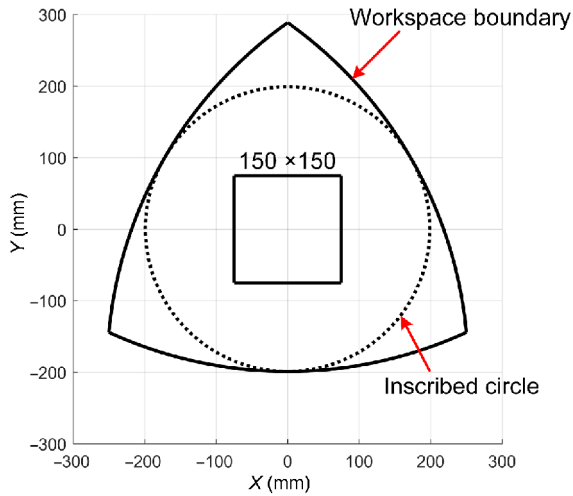


Figure 12 (Color online) Workspace of the 3-RRR parallel manipulator.

system is depicted in [Figure 13](#). The apparatus consists of an IPC (industrial personal computer), a motion control card, three AC servo systems, a 3-RRR PPM, and an online machine vision-aided system.

The IPC contains the control software programmed by C# language. The GALIL DMC-1886 motion control card is embedded on the PCI bus inside the IPC to realize the real-time control. The DMC-1886 motion control card also provides a communication driver library supported on the Windows, .NET and DOS platform, allowing the researcher to perform the secondary development. The command value is calculated and converted into the voltage signal by the specific algorithm, and the control signal is sent to servo systems through the PICM-2900D interconnection module. The 3-RRR PPM is driven by three independent Yaskawa servo systems. The electronic part of each rotating servo motor system is composed of a servo motor and an encoder, a servo driver and a limit switch which assists in returning home. The encoder can provide the real-time feedback to correct the rotation angle of the motor, which guarantees the input accuracy of the 3-RRR positioning system.

As shown in [Figure 14](#), the online vision-aided system is composed of a high-resolution camera, a lens with the focus length of 16 mm, light emitting diode (LED) markers and a high-performance computer used as an image processor. The main working principle of the system is to calculate the position and placement angle of central point of the active marker plate based on three LEDs. The software of the online vision-aided system is Halcon.

As the feedback device of the 3-RRR positioning system, the vision-aided measuring device must have high measurement accuracy. [Figure 15](#) presents 1010 times measuring results of the static end-effector using this machine vision-aided system. The repeated measurement accuracy in the X direction of the vision-aided system is within the range of

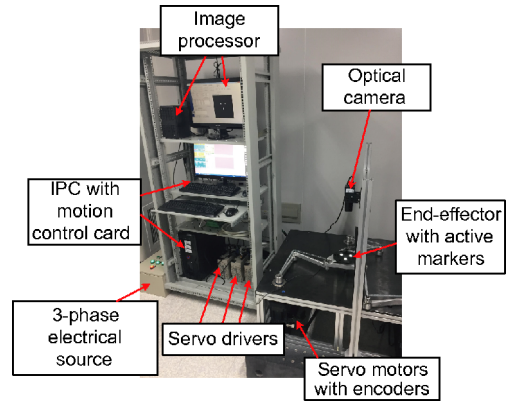


Figure 13 (Color online) The experimental setup of 3-RRR positioning system.

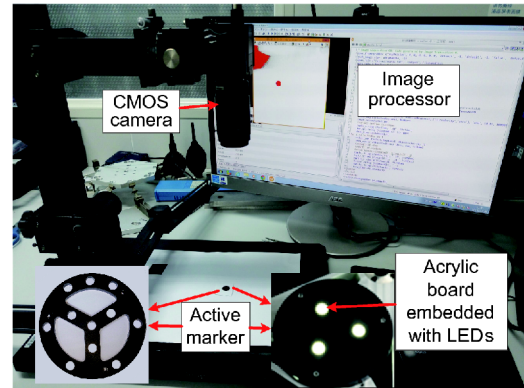


Figure 14 (Color online) Devices of the vision-aid system.

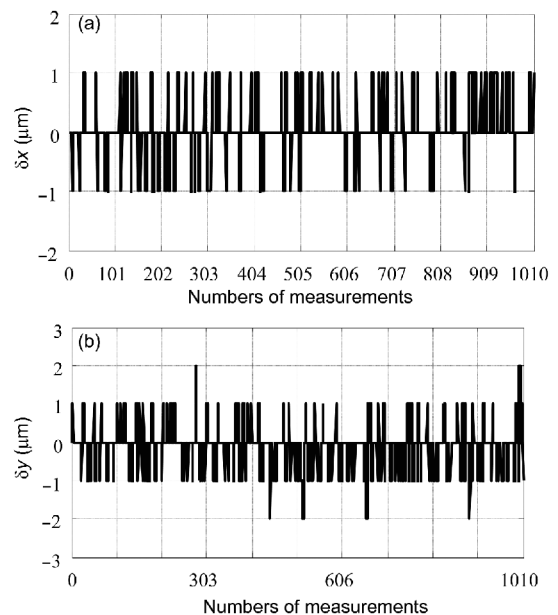


Figure 15 Repeated measurements of the vision-aid system. (a) Error in X direction; (b) error in Y direction.

$\pm 1 \mu\text{m}$, and the repeated measurement accuracy in the Y direction is within the range of $\pm 2 \mu\text{m}$. This indicates that the machine vision-aided system has high measurement accuracy, and the experiments are performed in a reliable and accurate way.

With the use of active markers, the processing time of the vision aid system for each frame is approximately 20 ms, which is up to 50 fps. In our experiments, because of the limitation of the camera data interface (GigeE), the acquisition speed is set at 30 fps, i.e., each visual servo period is approximately 33 ms. This processing speed is still fast, indicating that our vision aid system is qualified to be used in the real-time control of the 3-RRR positioning system.

Further informations of the experimental apparatus are listed in Table 3.

4.2 Experiments and discussion

The experiment procedure of the full-closed loop control is conducted as follows:

Step 1. Enter the terminal position of the end-effector $r(t)$ on IPC.

Step 2. According to the trajectory planning algorithm, the rotation angle with time is calculated. Next, the motion control card sends the corresponding control value to the servo drivers. Driven by servo motors, the end-effector of the 3-RRR PPM arrives at the desired position; this is defined as the first movement.

Step 3. The vision-aided system measures the actual position of the end-effector $y(t)$ and then sends the feedback to the IPC. Afterwards, the positioning error e and its first derivative e_c are obtained.

Step 4. The compensation is computed by the adaptive control algorithm.

Step 5. The motion control card sends the corresponding compensation value to the servo drivers. Driven by servo

motors, the end-effector of the 3-RRR PPM completes correction movement.

Step 6. Repeat Step 3 to Step 5 until the positioning error is less than the preset threshold.

According to the above procedure, the more adjustments the end-effector requires, the longer time the positioning system will require. Thus, the performance of the controller can be evaluated by the adjustment times.

We use five kinematic models as the control models to test the effectiveness and robustness of the proposed method. The first model is the theoretical kinematic model, whose parameters are shown in Table 4. To verify the effectiveness of the proposed control method for the 3-RRR PPM model, which has a time-varying property, the parameters of the theoretical kinematic model are modified randomly, and four modified kinematic models are obtained as shown in Table 5. All these control models are utilized in the experiments.

The thresholds of positioning errors are set as $x_e = 0.01 \text{ mm}$ and $y_e = 0.01 \text{ mm}$. Twenty-four test positioning points are selected inside the workspace of the 3-RRR PPM, and the test points is numbered as shown in Figure 16. Both the adjustment times of the 3-RRR PPM and its trajectory from home to each test positioning point are recorded.

For the theoretical control model, the number of adjustments are shown in Figure 17. According to Figure 17, under the proposed adaptive control the adjustment times of precise positioning to the test points are less than 2 times. This demonstrates that the positioning is of high efficiency.

To compare the performances of proposed control method, more experiments are conducted under the conventional PI control method. Usually, the parameters of PI controller are obtained by experimental parameter tuning. The experiments are conducted, and the suitable parameters K_p and K_i of the PI controller are obtained as 1. The adjustments to test positioning points are also less than 2 times. This indicates that, with the suitable control parameters, the conventional PI

Table 3 Description of experimental apparatus

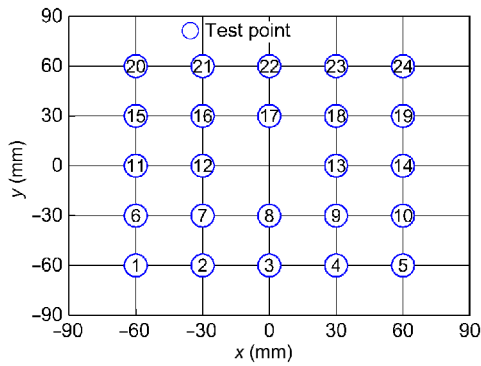
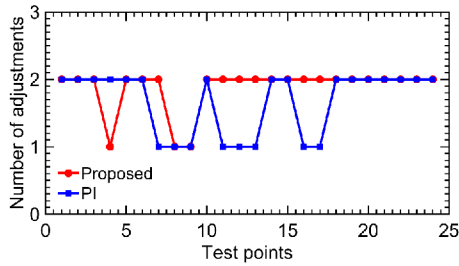
Name	Model	Description
Control card	GALIL DMC-1886	32-bit DSP, 8-axis motion control, 22 MHz feedback rate
Servo system	Yaskawa 7 series	3000 r/min speed with 24-bit encoder
CMOS camera	Tendency Dalsa Genie TS M2048	2048×2048 resolution
Lens	KOWA LM16SC	16 mm fixed focus
Software for programming and control	Microsoft Visual Studio 2015	Secondary development combined C# and GalilTools

Table 4 Parameters of the theoretical control model

	a	b	h	d
Chain 1	245.0	242.0	112.0	400.0
Chain 2	245.0	242.0	112.0	400.0
Chain 3	245.0	242.0	112.0	400.0

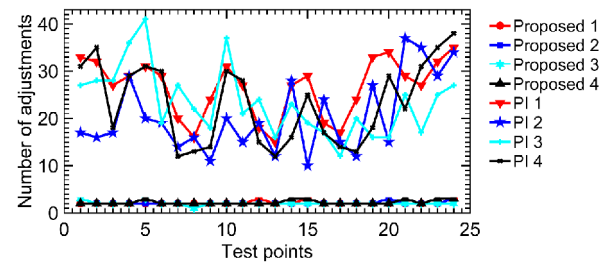
Table 5 Parameters of the modified control models

		a	b	h	d
Control model 1	Chain 1	243.0	242.0	110.0	400.0
	Chain 2	245.0	241.0	110.0	400.0
	Chain 3	245.0	241.0	110.0	400.0
Control model 2	Chain 1	243.0	241.0	110.0	400.0
	Chain 2	244.0	241.0	110.0	400.0
	Chain 3	243.0	240.0	110.0	400.0
Control model 3	Chain 1	243.0	241.0	110.0	400.0
	Chain 2	244.0	241.0	110.0	400.0
	Chain 3	243.0	240.0	110.0	400.0
Control model 4	Chain 1	244.0	241.0	110.0	399.0
	Chain 2	244.0	241.0	110.0	400.0
	Chain 3	243.0	240.0	110.0	400.0

**Figure 16** (Color online) Test point location.**Figure 17** (Color online) Numbers of adjustments for the theoretical model.

control method may have a good control performance based on the theoretical control model.

To evaluate the proposed control method with the stochastic modified control models, as shown in Table 5, further experiments are conducted. Moreover, keeping the same effective parameters of the PI controller as those in previous experiments, more experiments are also conducted with PI algorithm for the modified control models for the comparison. Figure 18 shows the adjustment times of the modified models using both the proposed method and the conventional

**Figure 18** (Color online) Efficiency comparison based on the modified model.

PI method. Experimental data for modified models 1, 2, 3, and 4 are plotted as groups 1, 2, 3, and 4, respectively. Figures 19 and 20 present the test point (30, 60) positioning trajectory for the modified model 1 based on the proposed method and the PI method, respectively, as examples.

According to Figure 18, using the proposed control method, the adjustments to all test points are less than 3 times. The smooth trajectory and precise final positioning can also be found in Figure 19. Although the first movement has approximately 150 μm error, the positioning error is less than 10 μm under the control of proposed method. This indicates that the 3-RRR positioning system still achieves excellent control performances using the proposed method. Although the parameters of the control model are changed, the proposed control method enjoys high efficiency and strong robustness.

Figure 20 shows that under the conventional PI control request, at least 12 times the adjustments are required, far greater than that under the proposed control. For further points, such as (60, -60), the number of adjustment times is even up to 41 times. From the overall and local trajectory in Figure 20, the error of the first movement is found out to be quite large. Though the end-effector can move quickly to the area nearby the test point after the first compensation, the

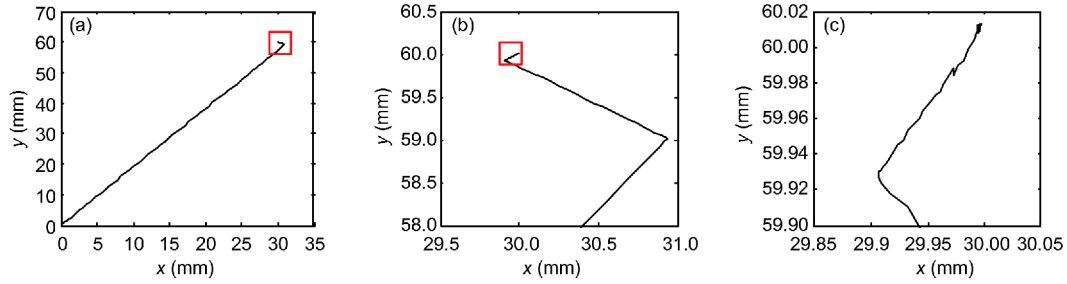


Figure 19 (Color online) The positioning trajectory based on the proposed adaptive control method (modified model). (a) The trajectory of the whole positioning movement; (b) the local trajectory; (c) the terminal trajectory.

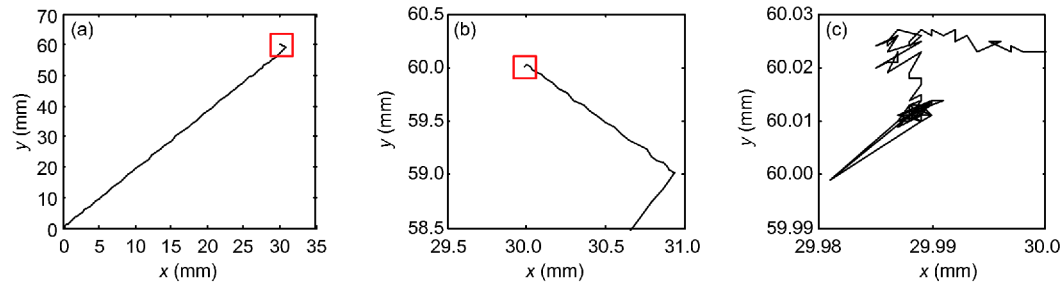


Figure 20 (Color online) The positioning trajectory based on the PI control method (modified model). (a) The trajectory of the whole positioning movement; (b) the local trajectory; (c) the terminal trajectory.

positioning error has not been less than the thresholds x_e and y_e after many adjustments. Finally, it takes 32 times of adjustments for the end-effector to finish precise positioning. Thus, the 3-RRR PPM takes a much longer time to complete the positioning under the conventional PI control. This longer time requirement is inefficient and impractical for the time-varying system.

These experimental results show that both control methods have similar control effects when the control model is determined and accurate, which is highly closed to the actual model of 3-RRR PPM. However, when the control model changes via some factors such as like motion wears or joint clearances, the proposed method shows its superiority over the conventional PI control method with very fewer adjustments and stable performance. This result proves that the proposed adaptive control method is suitable for the 3-RRR positioning system, which has the nonlinear and time-varying properties. Large-scale positioning also demonstrates the higher operability and robustness of the proposed control method. Moreover, as seen from the machine vision feedback, the final positioning error is within $10\ \mu\text{m}$, which is of high accuracy.

5 Conclusions

This paper presents an adaptive control method of the 3-RRR positioning system for the macro-micro combination system

based on machine vision aid. The setup of the 3-RRR positioning system is described in detail, including the kinematics modeling of 3-RRR PPM and online vision-aided system modeling. The experimental apparatus is also introduced clearly, and a series of experiments are conducted. Under the proposed control method, the 3-RRR positioning system shows higher stability, operability, and efficiency compared with the conventional PI control method. These experimental results demonstrate the high precision, effectiveness, and robustness of the proposed control, which is suitable for the time-varying PPM system. Furthermore, based on the proposed control method and machine vision-aided system, the positioning accuracy of the 3-RRR PPM is improved from approximately $\pm 150\ \mu\text{m}$ to $\pm 10\ \mu\text{m}$, which is smaller than the workspace of the micro positioner [5]. In other words, our 3-RRR positioning system based on monocular vision is capable as the macro part in the macro-micro combination positioning system. Therefore, the proposed method can make contributions to both the study of PPM control and the development of the macro-micro combination positioning system.

For further investigations, the dynamic control of the 3-RRR positioning system using acceleration feedbacks will be studied, and the macro-micro combination positioning system will be miniaturized for installation in a SEM.

Research Projects of Guangdong Province (Grant No. 2015090330001) and the Natural Science Foundation of Guangdong Province (Grant Nos. S2013030013355 & 2016A030310408).

- 1 Fatikow S, Eichhorn V, Krohs F, et al. Development of automated microrobot-based nanohandling stations for nanocharacterization. *Microsyst Technol*, 2008, 14: 463–474
- 2 Gupta R, Cavanah T M, Panhuis I H M. Nanomanipulation of individual carbon nanotubes. *Microsc Microanal*, 2004, 10: 962–963
- 3 Fahlbusch S, Mazerolle S, Breguet J M, et al. Nanomanipulation in a scanning electron microscope. *J Mater Process Technol*, 2005, 167: 371–382
- 4 Tran A V, Zhang X, Zhu B. The development of a new piezoresistive pressure sensor for low pressures. *IEEE Trans Ind Electron*, 2017
- 5 Wang R, Zhang X. Parameters optimization and experiment of a planar parallel 3-DOF nanopositioning system. *IEEE Trans Ind Electron*, 2018, 65: 2388–2397
- 6 Merlet J P. Jacobian, manipulability, condition number, and accuracy of parallel robots. *J Mech Des*, 2006, 128: 199–206
- 7 Gao F, Qi C K, Ren A Y, et al. Hardware-in-the-loop simulation for the contact dynamic process of flying objects in space. *Sci China Tech Sci*, 2016, 59: 1167–1175
- 8 Yao S, Zhang X, Yu J, et al. Error modeling and calibration of a 4RR redundant positioning system. *AIP Adv*, 2017, 7: 095009
- 9 Yu J J, Dai J S, Bi S S, et al. Type synthesis of a class of spatial lower-mobility parallel mechanisms with orthogonal arrangement based on Lie group enumeration. *Sci China Tech Sci*, 2010, 53: 388–404
- 10 Li Q, Wu F X. Control performance improvement of a parallel robot via the design for control approach. *Mechatronics*, 2004, 14: 947–964
- 11 Vivas A, Pognet P. Predictive functional control of a parallel robot. *Control Eng Pract*, 2005, 13: 863–874
- 12 Korayem M H, Tourajzadeh H, Taherifar M, et al. A novel method for recording the position and orientation of the end effector of a spatial cable-suspended robot and using for closed-loop control. *Int J Adv Manuf Technol*, 2014, 72: 739–755
- 13 Shang W, Cong S. Motion control of parallel manipulators using acceleration feedback. *IEEE Trans Contr Syst Technol*, 2014, 22: 314–321
- 14 Shang W W, Cong S, Ge Y. Adaptive computed torque control for a parallel manipulator with redundant actuation. *Robotica*, 2012, 30: 457–466
- 15 Yang H, Shao L, Zheng F, et al. Recent advances and trends in visual tracking: A review. *Neurocomputing*, 2011, 74: 3823–3831
- 16 Li H, Zhang X, Zhu B, et al. Micro-motion detection of the 3-DOF precision positioning stage based on iterative optimized template matching. *Appl Opt*, 2017, 56: 9435–9443
- 17 Wu H, Zhang X, Gan J, et al. High-precision displacement measurement method for three degrees of freedom-compliant mechanisms based on computer micro-vision. *Appl Opt*, 2016, 55: 2594–2600
- 18 Cheng H, Yiu Y K, Li Z. Dynamics and control of redundantly actuated parallel manipulators. *IEEE/ASME Trans Mechatron*, 2003, 8: 483–491
- 19 Yong Y K, Lu T F, Minase J. Trajectory following with a three-DOF micro-motion stage. In: Australasian Conference on Robotics and Automation. ACRA, 2006. 6–8
- 20 Ren L, Mills J K, Dong Sun J K. Trajectory tracking control for a 3-DOF planar parallel manipulator using the convex synchronized control method. *IEEE Trans Contr Syst Technol*, 2008, 16: 613–623
- 21 Vermeiren L, Dequidt A, Afroun M, et al. Motion control of planar parallel robot using the fuzzy descriptor system approach. *ISA Trans*, 2012, 51: 596–608
- 22 Wu J, Wang J, Wang L, et al. Dynamics and control of a planar 3-DOF parallel manipulator with actuation redundancy. *Mechanism Machine Theor*, 2009, 44: 835–849
- 23 Wu J, Wang D, Wang L. A control strategy of a two degrees-of-freedom heavy duty parallel manipulator. *J Dyn Sys Meas Control*, 2015, 137: 061007
- 24 Wu J, Wang J, You Z. An overview of dynamic parameter identification of robots. *Robot Comput Integr Manuf*, 2010, 26: 414–419
- 25 Wang D, Wu J, Wang L, et al. A method for designing control parameters of a 3-DOF parallel tool head. *Mechatronics*, 2017, 41: 102–113
- 26 Bonev I A, Gosselin C M. Singularity loci of planar parallel manipulators with revolute joints. In: Proceedings of the 2nd Workshop on Computational Kinematics. Seoul, 2001. 291–299
- 27 Gosselin C, Angeles J. The optimum kinematic design of a planar three-degree-of-freedom parallel manipulator. *J Mech Trans*, 1988, 110: 35–41
- 28 Liu X J, Jin Z L, Gao F. Optimum design of 3-DOF spherical parallel manipulators with respect to the conditioning and stiffness indices. *Mechanism Machine Theor*, 2000, 35: 1257–1267
- 29 Lepetit V, Moreno-Noguer F, Fua P. EPnP: An accurate O(n) solution to the PnP problem. *Int J Comput Vis*, 2009, 81: 155–166
- 30 Zhang Z. A flexible new technique for camera calibration. *IEEE Trans Pattern Anal Machine Intell*, 2000, 22: 1330–1334
- 31 Wang L X. A Course in Fuzzy Systems. Upper Saddle River, NJ: Prentice-Hall Press, 1999
- 32 Ziemer R E, Tranter W H, Fanin D R. Signals and Systems: Continuous and Discrete. Upper Saddle River, NJ: Prentice-Hall Press, 1998
- 33 Salas F G, Santibáñez V, Llama M A. Fuzzy-tuned PD tracking control of a 3-RRR parallel manipulator: Stability analysis and simulations. *Intell Autom Soft Comput*, 2014, 20: 159–182
- 34 Zhang X, Zhang X. A comparative study of planar 3-RRR and 4-RRR mechanisms with joint clearances. *Robot Comput Integr Manuf*, 2016, 40: 24–33